IOP Publishing Journal of Physics B: Atomic, Molecular and Optical Physics

J. Phys. B: At. Mol. Opt. Phys. **48** (2015) 244003 (9pp) doi:10.1088/0953-4075/48/24/244003

# Disentangling formation of multiple-core holes in aminophenol molecules exposed to bright X-FEL radiation

**V Zhaunerchyk[1,2], M Kamińska[2,3,4], M Mucke[2], R J Squibb[1,2,5], J H D Eland[1,2,6], M N Piancastelli[2,7], L J Frasinski[5], J Grilj[8], M Koch[8,9], B K McFarland[8], E Sistrunk[8], M Gühr[8], R N Coffee[8], C Bostedt[8], J D Bozek[8], P Salén[3], P v d Meulen[3], P Linusson[3], R D Thomas[3], M Larsson[3], L Foucar[10], J Ullrich[11,12], K Motomura[13], S Mondal[13], K Ueda[13], R Richter[14], K C Prince[14], O Takahashi[14], T Osipov[16], L Fang[16], B F Murphy[16], N Berrah[16,17] and R Feifel[1,2]**

[1] Department of Physics, University of Gothenburg, Gothenburg, Sweden
[2] Department of Physics and Astronomy, Uppsala University, Uppsala, Sweden
[3] Department of Physics, Stockholm University, Stockholm, Sweden
[4] Institute of Physics, Jan Kochanowski University, Kielce, Poland
[5] Blackett Laboratory, Imperial College London, London, UK
[6] Department of Chemistry, Oxford University, Oxford, UK
[7] LCPMR, UPMC and CNRS, Paris, France
[8] SLAC National Accelerator Laboratory, Menlo Park, CA, USA
[9] Institute of Experimental Physics, Graz University of Technology, Petersgasse 16, A-8010 Graz, Austria
[10] Max-Planck-Institut für medizinische Forschung, Heidelberg, Germany
[11] Max Planck-Institut für Kernphysik, Heidelberg, Germany
[12] Physikalisch-Technische Bundesanstalt, Braunschweig, Germany
[13] Institute of Multidisciplinary Research for Advanced Materials, Tohoku University, Sendai, Japan
[14] Elettra-Sincrotrone Trieste, Trieste, Italy
[15] Department of Chemistry, Hiroshima University, Japan
[16] Department of Physics, Western Michigan University, Kalamazoo, MI, USA
[17] Department of Physics, University of Connecticut, Storrs, CT, USA

E-mail: raimund.feifel@physics.gu.se

Received 14 August 2015, revised 22 September 2015
Accepted for publication 23 September 2015
Published 28 October 2015


**Abstract**

Competing multi-photon ionization processes, some leading to the formation of double core hole states, have been examined in 4-aminophenol. The experiments used the linac coherent light source (LCLS) x-ray free electron laser, in combination with a time-of-flight magnetic bottle electron spectrometer and the correlation analysis method of covariance mapping. The results imply that 4-aminophenol molecules exposed to the focused x-ray pulses of the LCLS sequentially absorb more than two x-ray photons, resulting in the formation of multiple core holes as well as in the sequential removal of photoelectrons and Auger electrons (so-called PAPA sequences).

Keywords: multiple ionization processes, double core hole, covariance mapping

(Some figures may appear in colour only in the online journal)

 

## 1. Introduction

About three decades ago Cederbaum and co-workers [1] investigated the formation of double core hole (DCH) states in molecules theoretically. Such states can be located either on one atomic site or on different atomic sites. The former case is often referred to as single-site (ss) DCH and the latter case as two-site (ts)-DCH. The study of ts-DCH states in molecules is of particular interest as they have been calculated to exhibit generally larger chemical shifts than the corresponding single core hole (SCH) states. This enhanced chemical sensitivity can be understood by the fact that the double ionization potential of ts-DCH states is linked to changes induced in the valence charge distribution at two different atomic sites [2]. The flow of the electron density between the atoms with inner-shell vacancies can be quantified in terms of the generalized inter-atomic relaxation energy.

Both kinds of DCH states in small molecules have recently been observed using synchrotron radiation [3–9]. In this case double ionization occurs upon absorption of a single photon and relies strongly on electron correlation. Subsequent to the early theoretical work of Cederbaum and co-workers [1], an alternative way of producing DCH states was pointed out by Santra and co-workers [10], in which two x-ray photons are absorbed by the molecule within a single ultra-short light pulse. Forming DCH states in this way became possible with the advent of the world's first x-ray free electron laser source, the Linac Coherent Light Source (LCLS) at SLAC, Stanford University, USA. This facility provides x-ray pulses of a few femtosecond (fs) duration. Such pulse lengths are necessary to successfully outdo the competing Auger electron emission which is a very fast decay process for inner shell vacancies of low-$Z$ elements. Ideally the x-ray pulses should be shorter than the lifetime of the $K$-shell vacancy to allow absorption of a second photon by the singly core-ionized molecule that occurs prior to the competing Auger decay.

Since the first lasing of the LCLS was obtained in 2009 [11], a series of experiments were carried out at the LCLS, proving the feasibility of probing DCH states in the Ne atom [12–14] and in several small molecules [15–19]. In the case of $N_2$, $N_2O$, CO, and $CO_2$ [18, 19] the experimentally measured values of DCH ionization potentials agree well with the theoretical predictions [2, 3, 20–23].

To unambiguously identify DCH states and their decay pathways, a multi-particle correlation spectroscopy technique should be advantageous. In contrast to conventional electron energy analyzers, a magnetic bottle spectrometer is characterized by an almost 100% electron collection efficiency at good energy resolution for comparatively high-energy electrons (up to several hundred eVs) and is fully multiplex (i.e. is capable of detecting simultaneously several charged particles created by the same light pulse) [24]. These features make the magnetic bottle spectrometer highly suitable for multi-electron correlation experiments. Since the LCLS operates at a low repetition rate of 120 Hz, while producing highly intense x-ray pulses, a single LCLS pulse may lead, on average, to a multitude of ionization events in the interaction volume, which severely limits the applicability of conventional coincidence analysis. To resolve this problem, the technique of covariance mapping [25, 26] can be employed as very recently demonstrated by us [13, 14, 27]. This method takes into account accidental events and thus reveals the true correlations.

In this work we elaborate on previous LCLS investigations of molecular DCH states by experimentally examining the more complex molecule of 4-aminophenol as proposed in the theoretical works of Santra *et al* [10] and Kryzhevoi *et al* [31]. The choice of this molecule should be regarded as an important step towards multiple inner shell ionization studies of even more complex (biomolecular) systems in condensed phase, in particular liquids and nano-crystals. We also examine the possibility that the 4-aminophenol molecules exposed to focused LCLS pulses of short duration (≈5 fs) may sequentially absorb more than two x-ray photons. In the light of this part of the study, we extend previous theoretical works [10, 31] to investigations of 4-aminophenol molecular states formed upon sequential absorption of three x-ray photons.

## 2. Experiment and data analysis

The experiments were carried out at the atomic, molecular and optical (AMO) science instrument [33] of the LCLS facility. The LCLS was operated in low-charge mode optimized nominally for an average x-ray pulse duration of about 5 fs at a repetition rate of 120 Hz. The LCLS was set to generate about 0.1−0.4 mJ radiation pulses at nominal photon energies of 354, 467, and 604 eV. Energies of the individual x-ray pulses were measured shot-by-shot with four different gas detectors upstream of the focusing optics.

As the LCLS is operated in the self-amplified spontaneous emission (SASE) mode, the radiation pulse energy varies from shot to shot with an estimated variation in the order of 15%. The x-ray pulses were focused with an elliptically bent Kirkpatrick–Baez pair of mirrors. To ensure the highest possible photon density on the target, as needed for nonlinear few-photon absorption processes, the FEL beam was focused to a spot size of ≈1 $\mu m^2$ providing peak intensities up to about $10^{17}$ W cm$^{-2}$. 4-aminophenol was evaporated by a heated oven source producing an effusive jet of target gas which was crossed with the x-ray beam. The 4-aminophenol used was a commercial sample of adequate (∼99%) purity as verified by examination of its mass spectrum. In order to detect efficiently the electrons ejected upon photon absorption we employed our custom-made 2 m long magnetic bottle time-of-flight (TOF) spectrometer FELCO [13, 14, 27, 29, 30], designed for multi-particle correlation studies at FEL sources. The resolving power of this instrument for single electrons, $E/\Delta E$, is about 50 for electron energies above 1 eV, and it has a fixed resolution $\Delta E$ of about 20 meV at lower energies. The average number of electrons produced by a single LCLS pulse was adjusted to be approximately 20−30. The complete analogue wave form of the TOF signals was recorded with 0.5 ns resolution at each laser shot and was sent to the central fast data storage of the

LCLS. Electron flight times were referenced to the FEL pulses. Electron kinetic energies, $E_{kin}$, were obtained after converting the TOF traces according to the formula

$$E_{kin} = \frac{D_0^2}{(t - t_0)^2} + E_0, \quad (1)$$

where $t$ stands for electron TOF and $D_0$, $t_0$ and $E_0$ are calibration constants [28]. These constants were found by calibrating the main $K$-shell lines and ss-DCH features to the values theoretically predicted by Kryzhevoi *et al* [31].

As outlined in the introduction, the ultra-intense LCLS pulses typically result in a large amount of ionization events implying that traditional coincidence measurements are not applicable for extracting electron pair correlations. To retrieve the correlations, we use instead the method of covariance mapping analysis [25, 26] that has previously been demonstrated by us to be highly suitable for the analysis of LCLS data [13, 14, 27]. In this method the covariance is calculated for electron signal intensities measured for a series of LCLS pulses. Fluctuations in the electron intensities under otherwise constant experimental parameter conditions obey the Poisson statistics implying that the covariance will be proportional to the intensity of correlated electron pair signals while it will be zero for uncorrelated electrons. The covariance maps are calculated as

$$\mathrm{Cov}(X, Y) = \langle XY \rangle - \langle X \rangle \langle Y \rangle, \quad (2)$$

where $X$ and $Y$ are the measured single-shot electron spectra and $\langle \ldots \rangle$ denotes averaging over the total number of x-ray shots. The LCLS pulse intensity, $I$, varies from shot to shot due to the SASE operation mode of the LCLS and due to instabilities of other machine parameters that will give rise to false correlations. To correct for contributions from fluctuating pulse intensities the technique of partial covariance mapping has been employed [13]

$$\mathrm{Cov}_p(X, Y) = \mathrm{Cov}(X, Y) - \frac{\mathrm{Cov}(X, I)\mathrm{Cov}(Y, I)}{\mathrm{Var}(I)}, \quad (3)$$

where $\mathrm{Var}(I) = \mathrm{Cov}(I, I)$ is the variance. Since in our case all the electrons are detected at a single detector, $X$ and $Y$ are the same, and hence the map is symmetric about the main diagonal, where intensity represents the variance. Several other corrections have been applied to the maps in order to correct for artificial correlation features associated with electronic noise, cable reflections and jitter in the x-ray photon energy (for further details see [14]).

## 3. Theoretical calculations

The molecular geometry of 4-aminophenol, schematically shown in figure 1, was calculated by geometry optimization at the MP2/cc-pVTZ level of theory using the Gaussian 09 suite of program [35]. Density functional theory (DFT) calculations of the SCH, DCH and other multiple core hole states were performed by the ΔKS method that allows computing the full relaxation of these states [34]. The basis set dependence of the

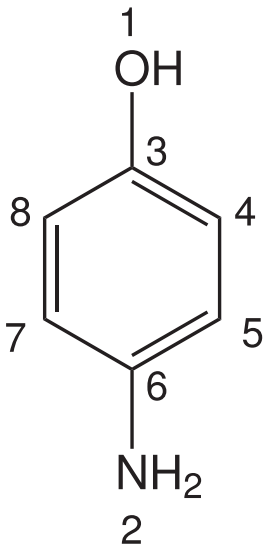


**Figure 1.** 4-aminophenol molecular structure.

**Table 1.** Theoretically calculated $K$-shell electron binding energies of SCH states compared with the calculations reported by Kryzhevoi *et al* [31] and experimental data obtained at the synchrotron radiation facility ELETTRA in Trieste [32]. The values in the table are given in eV. The carbon atoms are numbered in the same way as in figure 1.

| | This work (DFT) | Theory [31] | Experiment [32] |
|---|---|---|---|
| O | 538.89 | 538.26 | 539.2 |
| N | 405.29 | 404.87 | 405.4 |
| C3 | 291.41 | 291.59 | 291.4 and 291.1[a] |
| C4 | 289.71 | 290.25 | |
| C5 | 289.73 | 290.04 | |
| C6 | 290.97 | 291.20 | |
| C7 | 289.81 | 290.11 | |
| C8 | 289.93 | 290.18 | |

[a] SCH states for the C $K$-edge can resolve only two peaks.

DFT calculations was examined for the $K$-shell DCH states with the IGLO-III [37] and cc-pCVTZ [36] basis sets. The gradient-corrected exchange (PD86) [38] and correlation functional (PD91) [39] of Perdew and Wang were used for the correlation-exchange functional in the DFT calculations. All the DFT calculations were carried out using the STOBE-DEMON program [40].

## 4. Results and discussions

The following notation is used for describing the data: P($X$) is the photoelectron emitted from the $K$-shell of atom $X$ = C, N, O, and A(X) and V describe an electron associated with an Auger decay and valence ionization, respectively. Accordingly, sequential processes are denoted as, for instance, P(C)A (C), P(C)V, P(C)P(N) etc where the order is relevant. The additional notation of (ss) and (ts) is used to distinguish

**Table 2.** Theoretically calculated *K*-shell electron binding energies in eV. The table heading presents the ionization sequence and the electrons, for which the binding energies are listed, are denoted in bold. For comparison several binding energies taken from [31] are presented in parentheses. The carbon atoms are numbered in the same way as in figure 1. The ts-P**P**, PP**P** and (ss-PP)**P** binding energies for the six different carbon atoms are combined together and presented with '±' sign.

| | ss-P**P** | PA**P** | PAPA**P** | | ts-P**P** | | PP**P** | | (ss-PP)**P** |
|---|---|---|---|---|---|---|---|---|---|
| O | 625.37 (626.97) | 549.97 | 560.74 | CO | 544.21 ± 0.58 | CCO | 549.72 ± 0.88 | CCO | 549.76 ± 1.20 |
| N | 481.21 (482.30) | 416.71 | 427.85 | CN | 410.49 ± 0.55 | NCO | 548.60 ± 0.58 | NNO | 547.14 |
| C3 | 355.23 | 304.07 | 315.89 | ON | 409.38 (408.86) | CCN | 415.95 ± 0.81 | CCN | 416.02 ± 1.21 |
| C4 | 352.90 | 301.26 | 313.37 | CC | 296.53 ± 0.91 | OCN | 414.88 ± 0.61 | OON | 414.03 |
| C5 | 352.84 | 301.35 | 313.48 | OC | 295.58 ± 1.18 | CCC | 303.05 ± 1.19 | CCC | 302.75 ± 1.25 |
| C6 | 354.92 | 303.72 | 315.45 | NC | 295.47 ± 1.05 | OCC | 302.04 ± 1.32 | NNC | 300.66 ± 1.43 |
| C7 | 353.24 | 301.52 | 313.50 | | | NCC | 301.99 ± 1.19 | OOC | 300.99 ± 1.08 |
| C8 | 353.46 | 301.54 | 313.55 | | | ONC | 301.08 ± 1.31 | | |

ionization processes involving single and two atomic sites, respectively.

In table 1, our calculated *K*-shell electron binding energies of 4-aminophenol are given together with the previous results by Kryzhevoi *et al* [31] as well as with experimental data obtained in a separate study carried out at the synchrotron radiation facility ELETTRA in Trieste [32]. As can be seen, our theoretical values agree reasonably well with the experimental results, being lower by 0.3 eV for O, 0.1 eV for N, and by 1.4 eV for C. A similar tendency for the theoretical data to underestimate the experimental data is also observed for values reported by Kryzhevoi *et al*. Table 2 summarizes results of our theoretical calculations of 1s electron binding energies produced in various ionization sequences; more detailed data are given in the appendix of this paper. In general our results agree well with the predictions by Kryzhevoi *et al* for SCHs (table 1), while the agreement is less accurate for DCHs (table 2). The latter might be explained by the different sizes of the basis sets and the methods used.

Figures 2(a)–(c) show averaged electron spectra of 4-aminophenol recorded at the LCLS for the three nominal x-ray photon energies 354, 467 and 604 eV, respectively. The spectra were measured using weak (red lines) and strong (black lines) x-ray beam focusing conditions at the pulse duration of 5 fs. The photon energies were carefully chosen to be above each of the 1s ionization edges such that the resulting spectra of the ejected electrons show well resolved features. It is expected that for the spectra recorded under the focused beam condition contributions from nonlinear processes will be enhanced significantly. Indeed, the spectra recorded for different focus conditions (see figures 2(a)–(c)) exhibit substantially different peak shapes which can be regarded as first evidence for different ionization and relaxation processes occurring under the different experimental conditions. For example, the peak intensities associated with formation of SCHs, P(C), P(N) and P(O), are noticeably higher for the defocused x-ray beam reflecting the dominance of single-photon absorption processes with the defocused beam. Furthermore, apart from Auger hypersatellites (i.e. the first Auger electrons emitted by ss-DCH states) Auger electrons associated with multiple-photon absorption processes are expected to have smaller kinetic

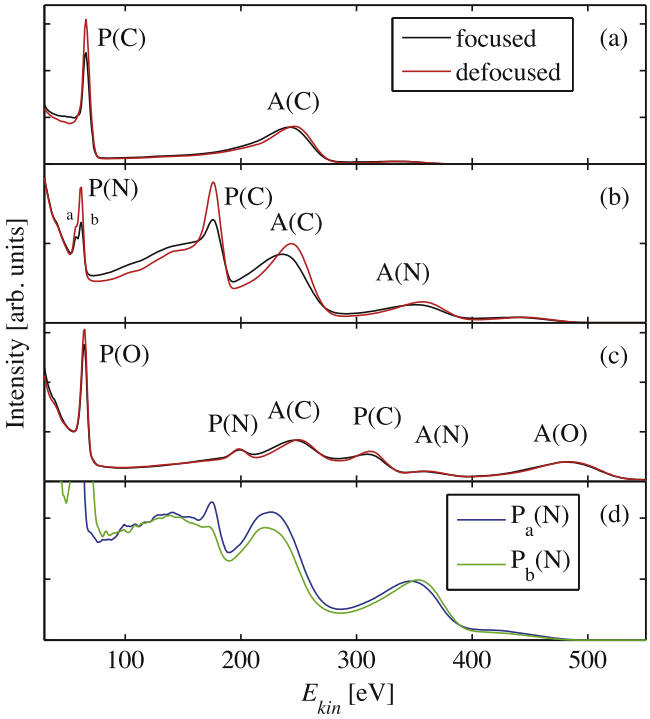


**Figure 2.** 4-aminophenol electron spectra for the $E_{\mathrm{kin}}$ range of 30 −550 eV measured under focused (black lines) and defocused (red lines) conditions at the photon energies of 354 eV (a), 467 eV (b), and 604 eV (c). The spectra are normalized to the total spectrum intensities. Panel (d) shows line profiles of the covariance map presented in figure 4(a) for the $E_{\mathrm{kin}}$ ranges of 53−59 eV and 59 −68 eV which are associated with $P_a$(N) and $P_b$(N), respectively, which are seen in panel (b).

energies compared with those from single photon reactions [2]. Such a tendency is also observed in figures 2(a)–(c), in which the shapes of the Auger peaks measured in focused beam conditions appear broadened and shifted towards lower kinetic energies. We note that the width of the photoelectron peaks is greater than the width expected from the intrinsic resolution of magnetic bottle spectrometer, $\Delta E/E \approx 2\%$, which implies that the experimental width of those peaks is most likely determined by the bandwidth of the LCLS photon beam.

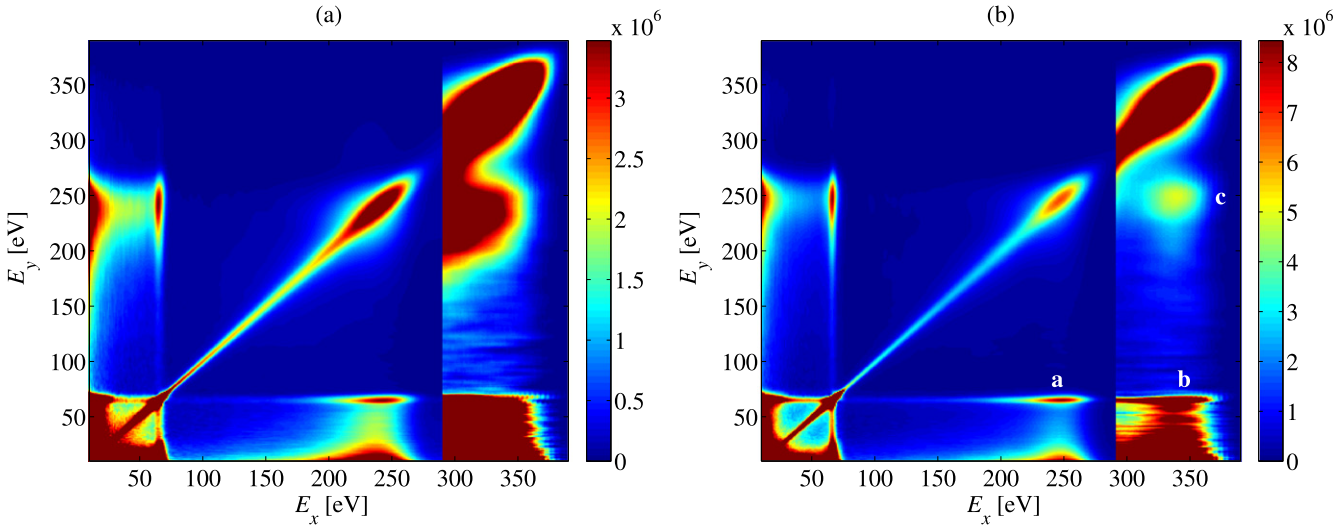


**Figure 3.** Covariance maps of 4-aminophenol electrons in the kinetic energy range of 10−390 eV obtained from data measured under focused (left) and defocused (right) beam conditions at the nominal photon energy of 354 eV. The maximum intensity of each map corresponds to the peak intensity of the P(C)A(C) island. For $E_x$ between 290 and 450 eV, the map was magnified 100 times to enhance the lower intensity features.

### *4.1. Ionization processes involving carbon inner shells (354 eV)*

Figure 3 displays two covariance maps which differ according to the degree of beam focusing. In both maps, apart from a distinct P(C)A(C) feature labelled 'a', one can also observe weak core-valence (P(C)V labelled'b'), and Auger-valence (A(C)V labelled 'c') correlation islands, both of which can only originate from few-photon absorption processes. With the defocused x-ray beam (see figure 3(b)), the A(C)V feature is well separated from other correlation islands while with the focused beam it is smeared out and does not exhibit a clear maximum. This feature could in principle originate from at least three different ionization sequences: VP(C)A(C), P(C)VA(C) or P(C)A(C)V. The P(C)VA(C) sequence is unlikely, since valence ionization has to compete with the much faster Auger process; however, this possibility cannot be ruled out completely. The valence electron formed in the alternative P(C)A(C)V process will have lower kinetic energy compared to the valence electron originating from VP(C) due to the stronger binding energy of the former. Therefore, it seems likely that under defocused beam conditions the A(C)V correlation island is dominated by contributions from the VP(C)A(C) process, while with the focused beam additional contributions from P(C)A(C)V and possibly other processes involving absorption of more than two photons are also relevant. Indeed, such a tendency is seen in figure 3, which shows that with the focused beam island 'b' is shifted towards lower kinetic energies for valence electrons. We note that the multiple photon absorption processes involving valence shell ionization such as PAVP, PVAP and VP have been observed by us previously in the case of neon atoms exposed to X-FEL radiation under similar conditions [14].

### *4.2. Ionization processes involving carbon and nitrogen inner shells (467 eV)*

A photon energy of 467 eV is sufficiently high to ionize the inner shells of nitrogen and carbon atoms and to generate multiple PA-sequences on C and N atoms as well as multiple core-holes, e.g. (ss, ts)-P(C)P(C), P(C)P(N), P(N)P(C) etc, whereas formation of ss-DCH on the N atom is energetically inaccessible (see table 2). The one-dimensional electron spectra obtained at $h\nu = 467$ eV is presented in figure 2(b). At this photon energy the cross section for ionizing the nitrogen *K*-shell is expected to be higher than that for the carbon *K*-shell. However, we note that the feature P(C) appears to be more intense than P(N), which we attribute to the fact that there are six times more carbon atoms in aminophenol than nitrogen and the cross section for carbon inner shell ionization should still be quite high. The spectrum of nitrogen Auger electrons occurs in the kinetic energy range of 300−400 eV and accompanies the already observed spectrum of carbon Auger electrons (200−280 eV).

The covariance maps of 4-aminophenol at the photon energy of 467 eV and at a pulse duration of 5 fs obtained under focused and defocused beam conditions are shown in figures 4(a) and (b), respectively. The single photon ionization processes P(C)A(C) and P(N)A(N) labelled 'd' and 'e', respectively, are clearly observed in both maps. However, with the focused x-ray beam, the covariance map shows a number of additional features that are not present in the map obtained with the defocused beam. One such feature, labelled 'f' in figure 4(a), is the correlation island formed by ≈100 −170 eV kinetic energy electrons and carbon Auger electrons with kinetic energies of 200−280 eV, and achieves the maximum intensity for C 1s photoelectrons at ≈153 eV. This feature can originate from different processes such as PA sequences [41] on carbon atoms and multiple core holes. Such

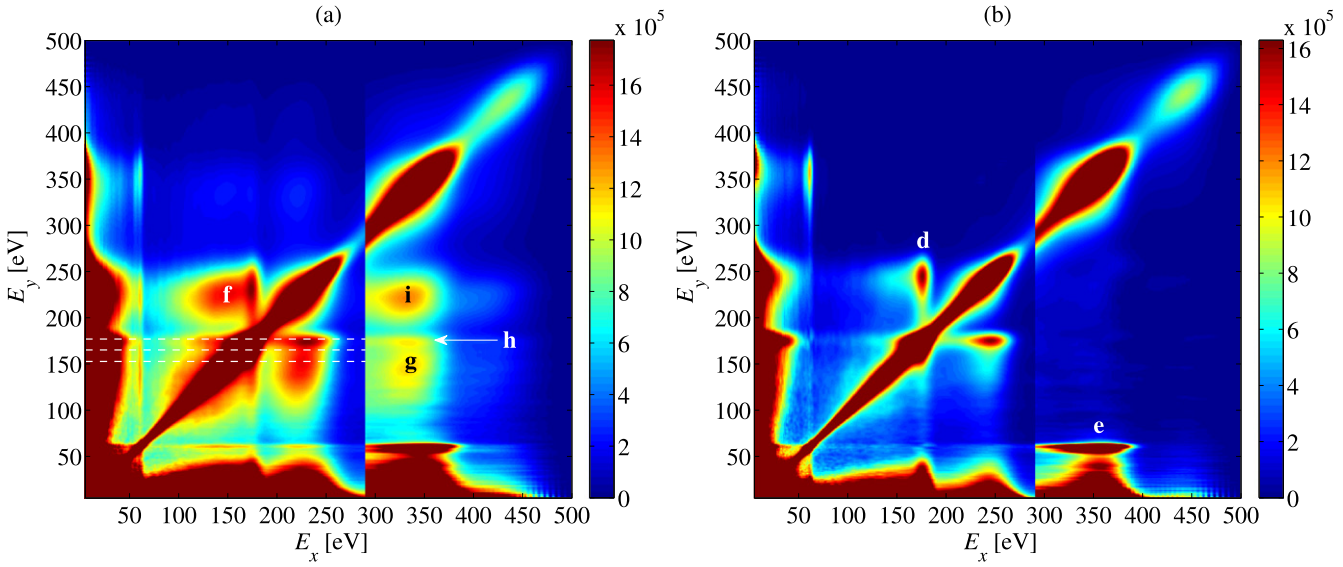


**Figure 4.** Covariance maps of 4-aminophenol electrons in the kinetic energy range of 10−500 eV obtained from data measured under focused (left) and defocused (right) beam conditions. The maximum intensity of each map corresponds to the peak intensity of the P(C)A(C) island. The 280−500 eV part was magnified five times to enhance the lower intensity features. In panel (a) the white dashed lines point on the *y*-axis to the kinetic energies of C 1s photoelectrons which are in decreasing order associated with **P**, PA**P**, and PAPA**P**.

sequential PA processes have been observed previously by us and others at the LCLS for neon atoms and small molecules (see e.g. [12–14, 18] and references therein). To get better insight into the origin of correlation island 'f', we refer to our theoretical calculations listed in table 2. The theoretical predictions imply that the process associated with ss-P(C)P(C) does not dominate, as, otherwise, island 'f' would have the P (C) peak intensity at ≈115 eV. The theoretical predictions also imply that a C 1s photoelectron emitted after completion of a PA cycle has ≈12 eV lower $E_{kin}$ compared with the preceding photoelectron. The dashed lines in figure 4(a) point on the *y*-axis to $E_{kin}$ of the **P**, PA**P**, and PAPA**P** C 1s photoelectrons. In the case of the PA processes, the PAPA**P** routes are more favorable as they have $E_{kin}$ close to the maximum intensity of the island which is at ≈153 eV. Table 2 also indicates that subsequent C 1s photoelectrons associated with multiple core holes located on different atoms differ by $E_{kin} \approx 6$ eV. Although we have not performed theoretical calculations for the processes involving absorption of more than three photons, we assume that a similar shift of ≈6 eV is also valid for multiple core holes. The latter implies that five-site quintuple core-hole needs to be created to give rise to the feature with the maximum intensity at ≈153 eV, though we believe creation of such states to be unlikely. Other processes that represent a mixture of multiple-core holes and PA sequences cannot be ruled out. However, due to the limited $E_{kin}$ resolution, contributions of individual processes cannot be distinguished and, thus, what types of multiple core holes and PA sequences dominate the reaction cannot be inferred unambiguously.

Other distinct features of the covariance map obtained with the focused x-ray beam are correlation islands of P(N) (≈62 eV) with P(C) at $E_{kin} = 100-180$ eV and A(C) at $E_{kin} = 200-250$ eV as well as correlation islands associated with Auger electrons of the nitrogen atom in the kinetic energy of 320−370 eV, which are magnified in the kinetic energy range 280−500 eV of the map and labeled 'g'–'i'. An assertion that these features are signatures of multiple-photon absorption processes is supported by the fact that they are absent from the covariance map obtained with a defocused x-ray beam.

It is interesting to note that the P(N) feature consists of two peaks which are denoted in figure 2(b) as $P_a$(N) and $P_b$ (N). Singly core-ionized $N_2$ molecules, which may have been present in form of residual background gas, could also give rise to the additional peak $P_a$(N). We also note that it coincides with the energy of the second photoelectron of the ts-P (C)P(N) sequence. In order to examine this feature in further detail, we present in figure 2(d) the $P_a$ and $P_b$ line profiles of the covariance map obtained with the focused beam by the blue and green curves, respectively. Apparently, the $P_a$ line profile shows strong correlations with other photoelectrons and Auger electrons emitted by 4-aminophenol which provide evidence that $P_a$ is a 4-aminophenol feature. It is interesting to note that the $P_a$ peak, in contrast to $P_b$, correlates with the main C 1s photoelectron. Such an observation strongly supports the interpretation that $P_a$ is likely to be a signature of the formation of the ts-P(C)P(N) double core vacancy, where the first core-hole is created on the C atom and the second one on the N atom.

### *4.3. Ionization processes involving carbon, nitrogen and oxygen inner shells (604 eV)*

Measurements were also carried out at the photon energy of 604 eV which is above the oxygen *K*-shell edge. Under these conditions SCHs formation on all atoms are possible, and various combinations of ts-DCH states are energetically accessible. However, ss-DCHs can be created only on the

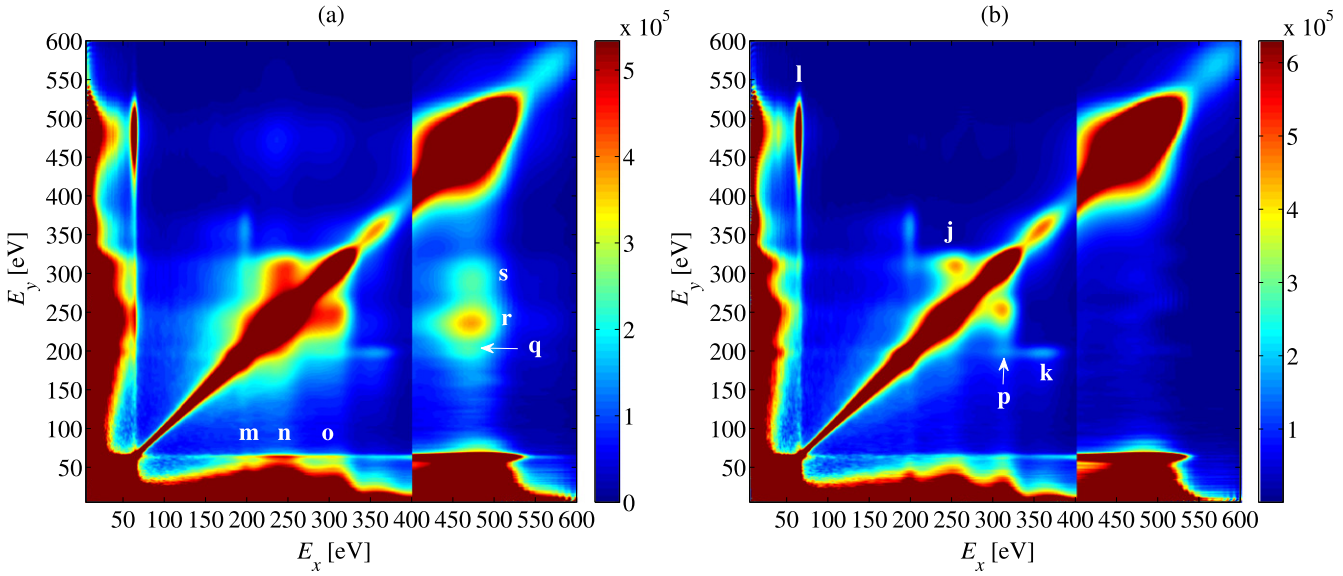


**Figure 5.** Covariance maps of 4-aminophenol for the electron kinetic energy range 10−600 eV obtained from data measured under focused (left) and defocused (right) beam conditons. The maximum intensity of each map corresponds to the peak intensity of the oxygen Auger electron island. The 400−600 eV part of the map was magnified five times to enhance lower intensity features.

carbon and nitrogen atoms, whereas the formation of an oxygen ss-DCH is energetically still not possible. Figure 2(c) represents the photoelectron spectra recorded at this photon energy. The most prominent feature at low kinetic energies is related to O 1s photoionization resulting in electrons in the kinetic energy range of 55 and 70 eV. The Auger electrons associated with decay of this SCH have kinetic energies in the range of 420 to 530 eV. In the 170−400 eV kinetic energy range of this spectrum there are four, almost equally spaced features which are attributed to the inner shell ionization of carbon and nitrogen and their subsequent normal Auger decay channels. Note that at this photon energy the carbon Auger electrons have lower kinetic energies compared to the carbon *K*-shell photoelectrons. The valence electrons are located above 550 eV and are not displayed in figure 2.

The corresponding covariance maps are shown in figure 5 where the cross correlation signals of all single photon ionization features are present in both maps; the P(C)A(C), P(N)A(N) and P(O)A(O) are labeled 'j', 'k' and 'l', respectively in this figure. The P(C)A(C) feature appears much broader and smeared out under focused conditions and is, therefore, attributed primarily to contributions from few-photon absorption processes discussed before. There is an additional weak feature at the energies of 290−315 eV and 190−210 eV labeled 'p' that is present in both maps. This feature seems to correspond to the correlation of the P(N) and P(C) signals and it might be due to the false correlations. However, ts-DCH and PA-sequences cannot be completely ruled out since the x-ray pulse intensity under defocused conditions may still have been sufficiently high to induce few-photon absorption processes.

Features possibly reflecting the ts-DCH states are correlation islands along the main P(O) line appearing at the crossings with P(N) ('m'), A(C) ('n') and P(C) ('o'), as well as the correlation islands located on the intersections of the A(O) signals (420−520 eV) with P(N)('q'), A(C) ('r'), and P(C) ('s'). The intensity of the 'm', 'n' and 'to' islands are higher on the covariance map measured with the focused beam which could be regarded as evidence for their origin from multi-photon absorption processes. The 'q', 'r', and 's'

**Table 3.** MVH, SCH, and ss-DCH ionization potentials. The values are given in eV units.

| MVH | | SCH | | ss-DCH | |
|---|---|---|---|---|---|
| VV | 20.75 | O | 538.89 | O | 1164.26 |
| VVVV | 67.95 | N | 405.29 | N | 886.50 |
| VVVVVV | 139.98 | C3 | 291.41 | C3 | 646.65 |
| VVVVVVVV | 238.28 | C4 | 289.71 | C4 | 642.61 |
| | | C5 | 289.73 | C5 | 642.56 |
| | | C6 | 290.97 | C6 | 645.90 |
| | | C7 | 289.81 | C7 | 643.05 |
| | | C8 | 289.93 | C8 | 643.40 |

**Table 4.** Ts-DCH ionization potentials. The values are given in eV units.

| | | | | | |
|---|---|---|---|---|---|
| ON | 948.27 | NC5 | 700.37 | C4C5 | 586.77 |
| OC3 | 836.60 | NC6 | 702.40 | C4C6 | 586.48 |
| OC4 | 834.03 | NC7 | 700.47 | C4C7 | 585.29 |
| OC5 | 833.39 | NC8 | 699.92 | C4C8 | 585.38 |
| OC6 | 834.87 | C3C4 | 588.00 | C5C6 | 587.59 |
| OC7 | 833.52 | C3C5 | 586.90 | C5C7 | 585.26 |
| OC8 | 834.39 | C3C6 | 588.40 | C5C8 | 585.40 |
| NC3 | 701.65 | C3C7 | 587.00 | C6C7 | 587.71 |
| NC4 | 699.71 | C3C8 | 588.21 | C6C8 | 586.69 |
| | | | | C7C8 | 586.70 |

**Table 5.** Ts-TCH ionization potentials. The values are given in eV units.

| | | | | | |
|---|---|---|---|---|---|
| ON | 1578.29 | C3C7 | 948.42 | C6C4 | 947.58 |
| OC3 | 1467.11 | C3C8 | 950.13 | C6C5 | 949.36 |
| OC4 | 1465.05 | C4O | 1192.58 | C6C7 | 949.52 |
| OC5 | 1464.10 | C4N | 1057.47 | C6C8 | 947.80 |
| OC6 | 1465.56 | C4C3 | 947.71 | C7O | 1191.73 |
| OC7 | 1464.29 | C4C5 | 946.18 | C7N | 1059.40 |
| OC8 | 1465.40 | C4C6 | 945.21 | C7C3 | 946.11 |
| NO | 1433.64 | C4C7 | 943.86 | C7C4 | 944.20 |
| NC3 | 1187.70 | C4C8 | 944.12 | C7C5 | 944.32 |
| NC4 | 1185.75 | C5O | 1191.13 | C7C6 | 947.86 |
| NC5 | 1186.86 | C5N | 1058.88 | C7C8 | 946.36 |
| NC6 | 1189.69 | C5C3 | 945.61 | C8O | 1193.63 |
| NC7 | 1186.98 | C5C4 | 946.16 | C8N | 1058.24 |
| NC8 | 1185.95 | C5C6 | 947.32 | C8C3 | 948.44 |
| C3O | 1198.43 | C5C7 | 943.94 | C8C4 | 944.67 |
| C3N | 1062.30 | C5C8 | 943.89 | C8C5 | 944.51 |
| C3C4 | 949.91 | C6O | 1195.21 | C8C6 | 945.96 |
| C3C5 | 948.27 | C6N | 1063.98 | C8C7 | 946.55 |
| C3C6 | 949.76 | C6C3 | 949.57 | | |

islands are undoubtedly nonlinear features as they appear only under focused conditions. However, due to the interplay of the two competing processes associated with ts-DCH formation and sequential PA-processes, whose contributions overlap on the covariance maps, these islands cannot be assigned unambiguously to solely one of the possibilities.

## 5. Conclusions

In this work we investigated the formation and decay of multiple 1s core holes in 4-aminophenol irradiated by powerful x-ray pulses delivered by the x-ray LCLS FEL source. The x-ray pulses were sufficiently short (≈5 fs) that multiple core holes could be created before Auger decays took place. Our data were acquired at three different photon energies in ascending order to open the core holes at C, N and O atomic species, respectively. By using covariance mapping and performing measurements at different x-ray pulse focusing conditions, we disentangled pairwise electron correlations associated with nonlinear processes. In order to obtain deeper insight into the origin of the observed nonlinear features, we performed DFT calculations. In particular, our theoretical calculations suggest that under the focused LCLS x-ray pulse conditions 4-aminophenol may sequentially absorb more than two photons. In general our theoretical results agree well with the earlier predictions by Kryzhevoi *et al* [31] for SCHs, while the agreement is less accurate for DCHs as shown in tables 1 and 2, respectively. The disagreement might be due to the different sizes of the basis sets and the methods used in the two different theoretical investigations.

We found that the experimental resolution of the data was not sufficient to separate contributions from individual multi-photon absorption processes, and the putative nonlinear features were observed to appear as the smearing out of the single-photon absorption features towards lower kinetic energy values. However, we note that they might also have a somewhat different origin. For example, long tails in the photoelectron distributions were observed before in atomic clusters exposed to strong FEL radiation [42], where they were explained by creation of a local plasma that affected the motion of photoelectrons and thereby the resolution of the experimental data. The formation of plasma under similar FEL conditions was found very recently to be general for extended systems [30, 43]. To what extent it can be active for the comparatively small aminophenol molecule remains a matter for separate, more elaborate, studies that we plan in the not too distant future.

**Table 6.** Ths-TCH ionization potentials. The values are given in eV units.

| | | | | | |
|---|---|---|---|---|---|
| ONC3 | 1251.33 | OC6C8 | 1136.61 | C3C4C7 | 890.58 |
| ONC4 | 1248.40 | OC7C8 | 1136.51 | C3C4C8 | 889.32 |
| ONC5 | 1248.39 | NC3C4 | 1003.26 | C3C5C6 | 890.87 |
| ONC6 | 1250.71 | NC3C5 | 1002.71 | C3C5C7 | 889.47 |
| ONC7 | 1248.74 | NC3C6 | 1004.99 | C3C5C8 | 888.30 |
| ONC8 | 1248.54 | NC3C7 | 1003.47 | C3C6C7 | 891.12 |
| OC3C4 | 1138.59 | NC3C8 | 1002.81 | C3C6C8 | 890.95 |
| OC3C5 | 1137.22 | NC4C5 | 1002.68 | C3C7C8 | 891.45 |
| OC3C6 | 1138.75 | NC4C6 | 1002.91 | C4C5C6 | 890.93 |
| OC3C7 | 1138.93 | NC4C7 | 1000.28 | C4C5C7 | 888.42 |
| OC3C8 | 1137.42 | NC4C8 | 1000.86 | C4C5C8 | 888.48 |
| OC4C5 | 1136.41 | NC5C6 | 1004.39 | C4C6C7 | 888.03 |
| OC4C6 | 1135.96 | NC5C7 | 1000.93 | C4C6C8 | 889.04 |
| OC4C7 | 1135.35 | NC5C8 | 1001.46 | C4C7C8 | 888.12 |
| OC4C8 | 1134.50 | NC6C7 | 1003.16 | C5C6C7 | 889.10 |
| OC5C6 | 1136.45 | NC6C8 | 1004.58 | C5C6C8 | 890.12 |
| OC5C7 | 1134.71 | NC7C8 | 1002.61 | C5C7C8 | 888.23 |
| OC5C8 | 1133.92 | C3C4C5 | 891.50 | C6C7C8 | 890.89 |
| OC6C7 | 1136.29 | C3C4C6 | 890.88 | | |

## Appendix

In this section we present our calculations performed with the DFT method for the ionization potentials of multiple valence holes (MVH), i.e. SCHs, ss-DCHs, ts-DCHs, ts-triple core hole (ts-TCH), and three site-TCHs (ths-TCHs). In tables 3–6 the numbers denote the atoms as they are labelled in figure 1.

## Acknowledgments

This work has been financially supported by the Swedish Research Council, the Göran Gustafsson Foundation (UU/KTH), and the Knut and Alice Wallenberg Foundation, Sweden. MKa acknowledges financial support from the Swedish Institute (SI). LJF and RJS thank the EPSRC, UK (Grant No. EP/I032517/1). KCP and RR acknowledge the MIUR, Italy (Grants No. FIRB-RBAP045JF2 and No. FIRB-RBAP06AWK3). KU and KM are grateful to MEXT for funding the x-ray Free Electron Laser Utilization Research Project and the x-ray Free Electron Laser Priority Strategy Program. SM is grateful to JSPS for financial support. NB, TO, LF, and BFM acknowledge financial support by the U.S. Department of Energy of Science, Basic Energy Science, Chemical, Geosciences, and Biological Divisions. JG acknowledges financial support by the European Union through the Marie Curie Actions. MKo acknowledges support by the Austrian Science Fund (FWF, Erwin Schrödinger Fellowship, J 3299-N20). MNP wishes to thank the French ANR (Agence Nationale de la Recherche) for partial support during her stay at the LCLS. Portions of this research were carried out at the LCLS at the SLAC National Accelerator Laboratory. LCLS is an Office of Science User Facility operated for the U.S. Department of Energy Office of Science by Stanford University.

## References

[1] Cederbaum L S *et al* 1986 *J. Chem. Phys.* **85** 6513
[2] Tashiro M *et al* 2010 *J. Chem. Phys.* **132** 184302
[3] Eland J H D *et al* 2010 *Phys. Rev. Lett.* **105** 213005
[4] Linusson P *et al* 2011 *Phys. Rev.* A **83** 022506
[5] Lablanquie P *et al* 2011 *Phys. Rev. Lett.* **106** 063003
[6] Lablanquie P *et al* 2011 *Phys. Rev. Lett.* **107** 193004
[7] Nakano M *et al* 2013 *Phys. Rev. Lett.* **110** 163001
[8] Hedin L *et al* 2014 *J. Chem. Phys.* **140** 044309
[9] Hedin L *et al* 2014 *Chem. Phys.* **439** 111
[10] Santra R, Kryzhevoi N and Cederbaum L S 2009 *Phys. Rev. Lett.* **103** 013002
[11] Emma P *et al* 2010 *Nat. Photonics* **4** 641
[12] Young L *et al* 2010 *Nature* **466** 56
[13] Frasinski L J *et al* 2013 *Phys. Rev. Lett.* **111** 073002
[14] Zhaunerchyk V *et al* 2013 *J. Phys. B: At. Mol. Opt. Phys.* **46** 164034
[15] Cryan J P *et al* 2010 *Phys. Rev. Lett.* **105** 083004
[16] Fang L *et al* 2010 *Phys. Rev. Lett.* **105** 083005
[17] Berrah N *et al* 2011 *Proc. Natl Acad. Sci.* 108 16912
[18] Salen P *et al* 2012 *Phys. Rev. Lett.* **108** 153003
[19] Larsson M *et al* 2013 *J. Phys. B: At. Mol. Opt. Phys.* **46** 164030
[20] Tashiro M, Ehara M and Ueda K 2010 *Chem. Phys. Lett.* **496** 217
[21] Takahashi O *et al* 2011 *J. Phys. Chem.* A **115** 12070
[22] Tashiro M, Ueda K and Ehara M 2011 *J. Chem. Phys.* **135** 15430
[23] Tashiro M, Ueda K and Ehara M 2012 *Chem. Phys. Lett.* **521** 45
[24] Eland J H D *et al* 2010 *Chem. Phys. Rev.* **485** 21
[25] Frasinski L *et al* 1989 *Science* **246** 1540
[26] Zhaunerchyk V *et al* 2014 *Phys. Rev.* A **89** 053418
[27] Mucke M *et al* 2015 *New J. Phys.* **17** 073002
[28] Eland J H D *et al* 2003 *Phys. Rev. Lett.* **90** 053003
[29] McFarland B K *et al* 2014 *Nat. Commun.* **5** 4235
[30] Murphy B F *et al* 2014 *Nat. Commun.* **5** 4281
[31] Kryzhevoi N, Santra R and Cederbaum L S 2011 *J. Chem. Phys.* **135** 084302
[32] Mucke M *et al* manuscript in preparation
[33] Bozek J 2009 *Eur. Phys. J. Spec. Top.* **169** 129
[34] Takahashi O and Pettersson L G M 2004 *J. Chem. Phys.* **121** 10339
[35] Frisch M J *et al* 2010 Gaussian 09, Revision B.01, (Wallingford, CT: Gaussian, Inc)
[36] Kutzelnigg W *et al* 1990 *NMR-Basic Principles and Progress* (Heidelberg: Springer)
[37] Woon D E and Dunning J T H 1993 *J. Chem. Phys.* **98** 1358
[38] Perdew J P and Yue W 1986 *Phys. Rev.* B **33** 8800
[39] Perdew J P and Wang Y 1992 *Phys. Rev.* B **45** 13244
[40] Hermann K *et al* 2011 StoBe-deMon version 3.1
[41] Rohringer N and Santra R 2007 *Phys. Rev.* A **76** 033416
[42] Bostedt C *et al* 2010 *New J. Phys.* **12** 083004
[43] Tachibana T *et al* 2015 *Sci. Rep.* **5** 10977